energies

MDPI

Article

An Experimental Study of an Autonomous Heat Removal System Based on an Organic Rankine Cycle for an Advanced Nuclear Power Plant

Nicolas Tauveron [1,*], Guillaume Lhermet [1,2], Benoît Payebien [1], Nadia Caney [1] and Franck Morin [2]

[1] Université Grenoble Alpes, CEA, LITEN, LCST, F-38054 Grenoble, France; benoit.payebien@cea.fr (B.P.)
[2] CEA, DES, DER, SESI, F-13108 Saint Paul Lez Durance, France
* Correspondence: nicolas.tauveron@cea.fr; Tel.: +33-4-38-78-61-51

Abstract: The present study focuses on the recovery of waste heat in an autonomous safety system designed for advanced nuclear reactors. The system primarily relies on passive safety condensers, which are increasingly integrated into the design of advanced Pressurized Water Reactors (PWRs). These condensers are typically immersed in large water tanks that serve as heat sinks and are placed at sufficient heights to ensure natural circulation. Such a heat removal system can operate for an extended period, depending on the size of the tank. This research is driven by the potential to recover part of the energy stored in the boiling water volume, using it as a heat source for an Organic Rankine Cycle (ORC) system via an immersed heat exchanger. The electricity generated by the ORC engine can be used to power the system components, thereby making it self-sufficient. In particular, a pump replenishes the water tank, ensuring core cooling for a duration no longer limited by the water volume in the tank. An experimental test setup, including a boiling water pool and an ORC engine with an electrical output of approximately several hundred watts, along with an immersed evaporator, was constructed at CEA (Grenoble, France). Several test campaigns were conducted on the experimental test bench, exploring different configurations: two distinct ORC working fluids, cold source temperature variation effects, and relative positioning of the submerged evaporator and heat source within the water tank impact. These tests demonstrated the reliability of the system. The results were also used to validate both the ORC condenser and evaporator models. This article presents this innovative system, which has recently been patented. Moreover, to the best of our knowledge, the investigated configuration of an ORC that includes an immersed evaporator is original.

Keywords: safety; organic rankine cycle; safety condenser; autonomous system

Citation: Tauveron, N.; Lhermet, G.; Payebien, B.; Caney, N.; Morin, F. An Experimental Study of an Autonomous Heat Removal System Based on an Organic Rankine Cycle for an Advanced Nuclear Power Plant. *Energies* **2024**, *17*, 5069. https://doi.org/10.3390/en17205069

Academic Editor: Marco Di Bartolomeo

Received: 11 September 2024
Revised: 3 October 2024
Accepted: 8 October 2024
Published: 11 October 2024

1. Introduction

With approximately 450 nuclear power plants (NPPs) in operation, nuclear energy generates around 10% of the world's electricity [1,2]. Over the past five decades, three major nuclear accidents have occurred: Three Mile Island (1979), Chernobyl (1986), and Fukushima Daiichi (2011) [3–5]. Lessons learned from these accidents have been incorporated into the design of new-generation NPPs (Generation III and beyond) with the aim of improving safety. As a result, safety enhancement programs have been developed, focusing on passive safety systems for these new reactors. These systems are designed to cope with extreme conditions, such as an extended loss of offsite power leading to a global loss of heat sink events, and they are capable of operating during a station blackout (SBO).

Passive systems, such as the passive residual heat removal system (PRHRS), derive their robustness from the absence of rotating machinery, such as pumps or diesel generators. Instead, they rely solely on natural forces, like natural convection, to transfer residual heat from the reactor core to a cold source, typically a water tank or air. The use of passive systems simplifies the plant's overall design, as well as its operation and maintenance [6].

Some new-generation NPPs already incorporate the PRHRS [7]. This system can be directly connected to the primary loop, as seen in the AP1000 [8] or CAP1400 [9] reactors. In these cases, the PRHRS transfers residual heat from the reactor core to a condenser pool via a heat exchanger (HX). To ensure natural convection, the condenser pool is placed above the reactor. Another approach is to connect the PRHRS through the secondary loop to cool the steam generator (SG), which removes decay heat from the primary loop, as in the HPR1000 [10]. This configuration is known as the secondary-side passive residual heat removal system (SSPRHRS). Since the SSPRHRS is connected to the secondary side, the PRHRS heat exchanger functions as a safety condenser (SACO). Some recent Small Modular Reactor (SMR) designs also include PRHRS systems [11].

Another safety concern raised by various regulatory authorities is the reliance on an emergency power supply in addition to existing power sources [12]. One proposed concept is to utilize the water tank as a heat source for a thermodynamic cycle, such as an Organic Rankine Cycle (ORC) engine. Other waste heat recovery systems could also serve as viable alternatives to the ORC. Notable options include Stirling engines, thermoelectric devices, and supercritical CO_2 Brayton cycles. Thermoelectric devices are appealing due to their simplicity and robustness, but they are not well-suited for temperature gradients below 100 °C. Stirling engines also present interesting opportunities; however, the associated heat exchangers between water and gas tend to be quite large, making them incompatible with the dimensions of the safety condenser (SACO). The supercritical CO_2 Brayton cycle has been investigated in various projects for nuclear decay heat removal situations [11], particularly in more favorable thermal conditions, where heat is extracted closer to the primary circuit. In these cases, the operating temperatures are higher, making the supercritical CO_2 Brayton cycle a promising option. However, this may not hold true for heat at 100 °C, taken from a location far from the primary circuit, which is preferable from a safety perspective. Additionally, the cold temperature in the sCO_2 cycle poses a significant challenge due to the critical temperature of CO_2, which falls within the range of 15 °C to 40 °C. The resulting very high pressure within the supercritical heater could also be a challenging problem.

Figure 1 illustrates the coupling between a passive residual heat removal system (PRHRS) and an Organic Rankine Cycle (ORC) engine. Components (1)–(6) are part of the primary circuit of a Pressurized Water Reactor (PWR), while the part numbered (7) represents the containment structure. The safety condenser, immersed in the condenser pool (9), is labeled as (8). The electricity generated by the ORC system ((10)–(13)) will not only power its own components, such as the pump, but will also provide a surplus of electricity for other uses [13,14]. This additional electricity will be utilized to pump water from a lower section (14) to the condenser pool (9), thereby allowing the core to be cooled independently of the volume of water above it; the corresponding pump is indicated as (15).

The Organic Rankine Cycle (ORC) is a thermally driven power cycle that generates electricity by utilizing a heat source and a low-boiling-point fluid as the working fluid [15,16]. The ORC engine has been identified as one of the most efficient thermal engines for producing electricity from low-temperature heat sources (typically below 150 °C) [17]. Most heat sources used for ORC systems are geothermal, with approximately 3 GW of cumulative installed capacity as of 2020, and power outputs ranging from a few kW to several dozen MW [18].

In Figure 1, components (10)–(13) represent the four key components of an Organic Rankine Cycle, functioning as follows: the working fluid is heated in an evaporator (10) by boiling water from the water tank (9). This high-temperature and high-pressure organic vapor is then expanded in a turbine (11), generating mechanical power that is converted into electricity by an electrical generator. Before returning to the pump, the low-pressure organic vapor is condensed in a condenser (12) linked to a cold source. Subsequently, the fluid is pumped back to a high-pressure level by a pump (13).

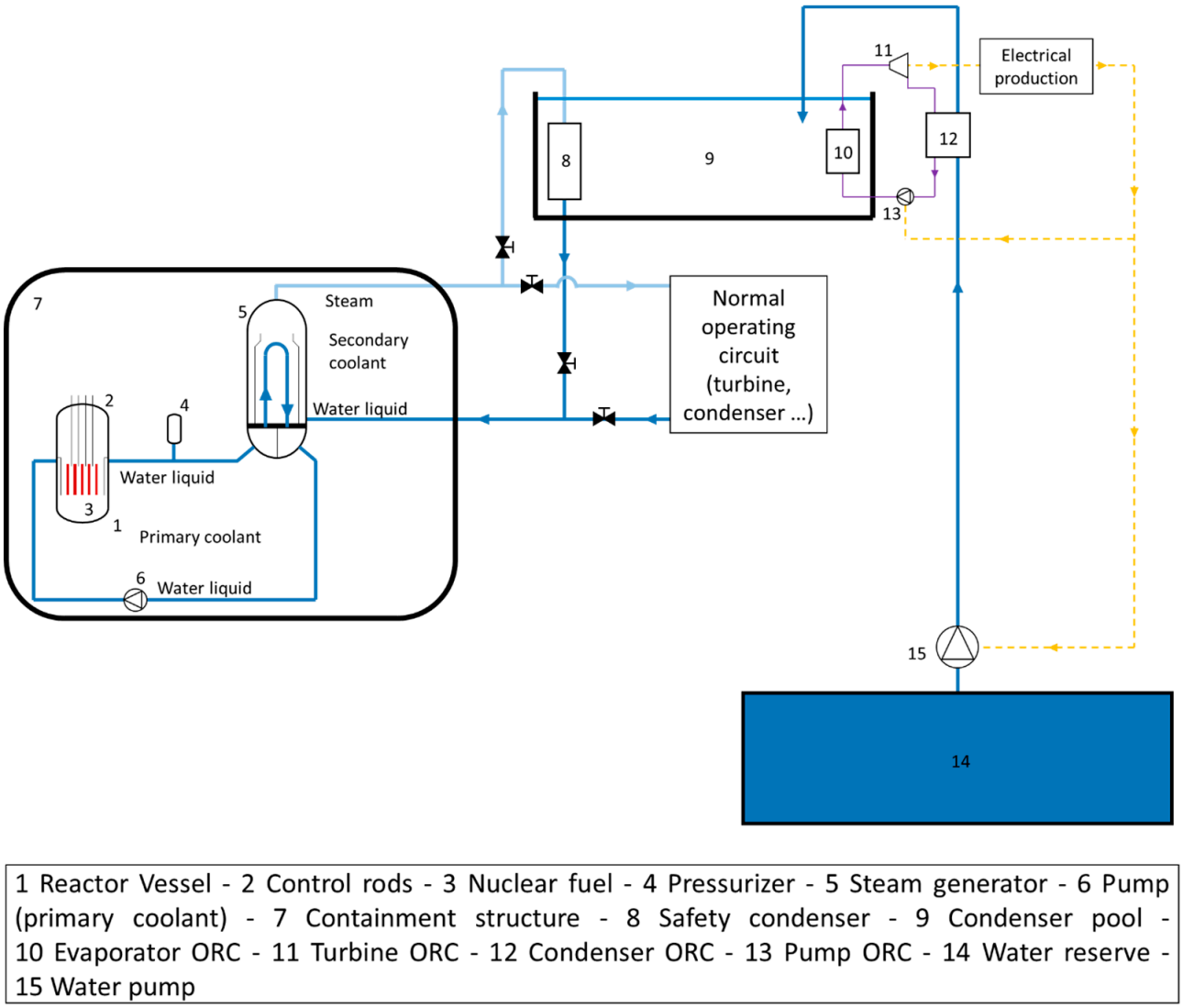

Figure 1. PRHRS and ORC engine coupling—simplified diagram (arrows correspond to the different fluid flows).

Regarding power levels, some next-generation reactors, such as the European Pressurized Reactor (EPR), are equipped with four steam generators (SGs). The residual power to be removed is approximately 1% of the nominal core power, which translates to about ten megawatts per SG, 24 h after reactor shutdown, a typical period during which the system is expected to be operational. Therefore, to maintain a constant water level in the condenser pool (due to evaporation), the ORC system must be capable of producing 5 kW. The main characteristics of the overall system are summarized in Table 1.

The objective of this work is to study, at a reduced scale, the reliability of the coupling between an Organic Rankine Cycle (ORC) engine and a water tank used as both a cold source for the passive residual heat removal system (PRHRS) and a hot source for the thermodynamic engine. This experimental study aims to validate thermal models that will be used to design the final full-scale system. The complete development of the model is not the focus of the present article; rather, it concentrates on the development and validation of the evaporator and condenser models.

Table 1. Typical characteristics of a PRHRS–ORC engine coupling.

Parameters	Unit	Value
SACO power (Heat source power)	[MW]	10
SACO Area	[m^2]	100
Tank Volume	[m^3]	375
Water tank temperature conditions	[C]	~100
ORC Immersed Evaporator Power	[kW]	200
ORC electrical power	[kW]	5
Resulting Ratios	**Unit**	**Value**
SACO power/Tank Volume	[kW/m^3]	27
SACO Heat flux	[W/cm^2]	~10
ORC Evaporator Power/SACO power	[-]	0.02
ORC electrical power/ORC Evaporator Power	[-]	0.025

The evaporator employed is an unconventional type for ORC systems: a tubular evaporator submerged within the boiling water tank, enhancing the integration between the ORC engine and the water tank. Natural convection is utilized to transfer heat from the boiling water to the outer walls of the tubes. Mini-channel-type tubes have been selected to maximize the heat transfer surface area while maintaining acceptable heat transfer coefficients inside the tubes. These small tubes, with a diameter of 3.2 mm, are widely used for heat dissipation in confined spaces [19]. A specific investigation into this type of evaporator is conducted in this article.

Moreover, although the ORC engine is a well-established system, its application in the context of nuclear safety necessitates a focus on reliability. The ORC engine must be capable of continuously producing electricity under all circumstances. In particular, adapting nuclear power plants to cope with high-temperature episodes exacerbated by climate change is a known concern for nuclear safety authorities [20,21]. Consequently, the temperature of the ORC engine's cold source (boiling water from the reservoir) is a critical factor to consider in reliability studies. A preliminary experimental campaign has addressed this issue, and the results will be used to validate the numerical model of the ORC condenser, which is the most affected component under varying cold source conditions.

Two additional experimental test campaigns in off-design configurations have also been identified:

- The second campaign investigates the position of the ORC engine's immersed evaporator within the condenser pool. The key question is whether the positioning of the evaporator relative to the heating elements influences its performance. This consideration is crucial for design, as the safety condenser (SACO) has stringent constraints, and the immersed evaporator should not adversely affect its behavior.
- The third campaign explores the use of alternative working fluids in the Organic Rankine Cycle. The selection of the most appropriate organic working fluid is a central issue in ORC system design. This choice generally involves a trade-off among various criteria (performance, cost, regulatory compliance, safety, etc.), and at this stage of the project, a final decision cannot be made. Consequently, several fluids must be studied. In this paper, two different fluids have been experimentally investigated, and numerical models based on non-dimensional parameters have been developed to facilitate their application to the future selected fluid, which may differ from those experimentally tested.

Section 2 presents the experimental setup. As previously mentioned, this work examines a completely innovative system that has recently been patented. Models for the condenser and evaporator have been developed (Sections 3.1 and 3.2, respectively). To the best of our knowledge, the configuration of an Organic Rankine Cycle (ORC) incorporating an immersed evaporator is original. Consequently, a dedicated heat transfer model is required. We have opted for a semi-empirical approach (Section 3.2.3). Following the

presentation of the nominal design point (Section 4.1), a specific study was undertaken to assess the system's robustness against variations in cold temperatures. A theoretical model has been developed and validated against experimental data (Section 4.2). Other critical parameters for the design study include the relative positioning of the heating elements and the immersed evaporator, as well as the choice of refrigerant (Section 4.3). Experimental campaigns have been conducted to explore these questions.

2. Experimental Test Bench

2.1. ORC Engine

The experimental test bench is composed of two main parts:

- The ORC engine circuit, which consists of four key components:
  - An immersed evaporator;
  - A partial admission axial micro-turbine;
  - A plate condenser;
  - A volumetric pump.
- The boiling water tank, designed to simulate the SACO pool, contains heating rods designed to play the role of the passive SACO system.

The purpose of the test bench is to serve as a small-scale demonstrator, with the results obtained used to validate the numerical models. The main characteristics of the demonstrator are summarized in Table 2.

Table 2. Characteristics of the test bench.

Parameters	Unit	Value
Heating rod power (Heat source power)	[kW]	80
Heating rod rode area	[m^2]	1
Tank Volume	[m^3]	1.5
Water tank temperature conditions	[C]	~100
ORC Immersed Evaporator Power	[kW]	7.5
ORC electrical power	[kW]	0.15
Resulting Ratios	**Unit**	**Value**
Heating rod power/Tank Volume	[kW/m^3]	53
Heating rod heat flux	[W/cm^2]	10
ORC Evaporator Power/Heating rod power	[-]	0.09
ORC electrical power/ORC Evaporator Power	[-]	0.02

Due to project constraints, it was not possible to maintain constant volumes and power levels between the full-scale configuration and the test bench. However, efforts were made to maintain similar system behavior by keeping the tank temperature conditions constant and preserving the same order of magnitude for key parameters. In particular, we aimed to keep four ratios constant: the heating rod power to tank volume, the heating rod heat flux, the ORC immersed evaporator to "hot source power", and the ORC electrical power to ORC immersed evaporator ratios. A comparison between Tables 1 and 2 highlights that the most significant difference lies in the ORC evaporator power to heating rod power ratio, as it was not feasible to sufficiently reduce the ORC evaporator power or significantly increase the heating rod power. Section 4.3 shows that when this ratio falls below 0.1, the overall system behavior remains unaffected.

At the inlet of the volumetric pump, the organic working fluid is in liquid form. The volumetric pump increases the working fluid's pressure to a high level before it is evaporated through an immersed evaporator. This organic vapor is then expanded in a partial admission axial micro-turbine, and a generator converts the mechanical energy into electricity. The low-pressure organic vapor is condensed using a plate condenser, which utilizes an external active water circuit as a cold source and is then recirculated back to the pump.

The system's lubrication is provided by the organic working fluid itself. A dedicated external circuit ensures the generator's cooling. A small centrifugal pump is placed just before the volumetric pump to slightly increase the pressure and prevent cavitation. A tank located between the condenser and the centrifugal pump ensures an adequate net positive suction head (NPSH) at the centrifugal pump inlet. An additional system, comprising a heat exchanger and a bypass mechanism, enables a wide range of cold source temperature studies. The combination of the pump and a needle valve facilitates the exploration of a wide range of mass flow rates and pressures.

The boiling water tank has a capacity of 1.5 m^3 and is equipped with ten 20 kW heating rods. Each heating rod has a heat flux density of 10.1 W/cm^2, which is similar in magnitude to that of the SACO system [22]. The heat rate in the pool can be adjusted between 0 kW and 80 kW, with a maximum of four heating rods in operation.

Figure 2 presents a picture of the coupling between the ORC engine and the boiling water tank. The test bench is a small-scale demonstrator for model validation purposes. The characteristics of the plate condenser and the immersed evaporator are provided in Tables 3 and 4.

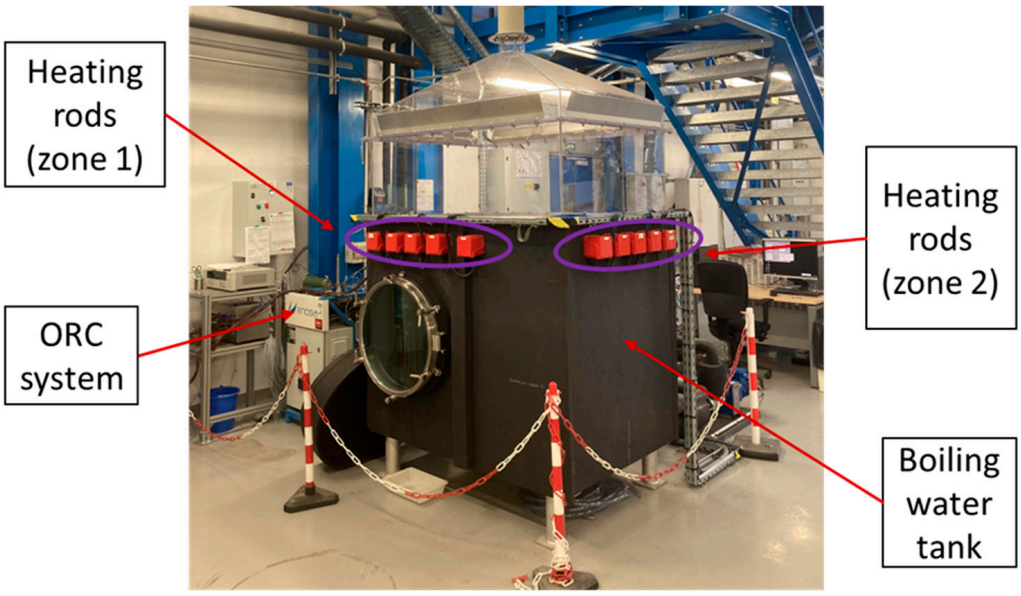

Figure 2. Coupling of the ORC engine and the boiling water tank.

Table 3. Characteristics of the plate condenser.

Parameters	Unit	Value
Type	[-]	Brazed plates
Model	[-]	SWEPB12H
Number of plates	[-]	40
Height	[mm]	287
Width	[mm]	117
Number of passes	[-]	1

Temperature sensor rods are used to measure the temperature gradient within the tank. The positioning of these rods in the water tank is shown in Figure 3. A level sensor system connected to an automatic valve regulates the water level in the tank.

Thermal losses were neglected in this study due to the moderate temperatures involved. However, all pipes and the main section of the boiling water pool were thermally insulated.

Table 4. Characteristics of the immersed evaporator.

Parameters	Unit	Value
Height	[mm]	800
Tube spacing (edge to edge)	[mm]	18
Tube diameter	[mm]	3.17
Tube thickness	[mm]	0.89
Number of tubes	[-]	551
Evaporator diameter	[mm]	406.4

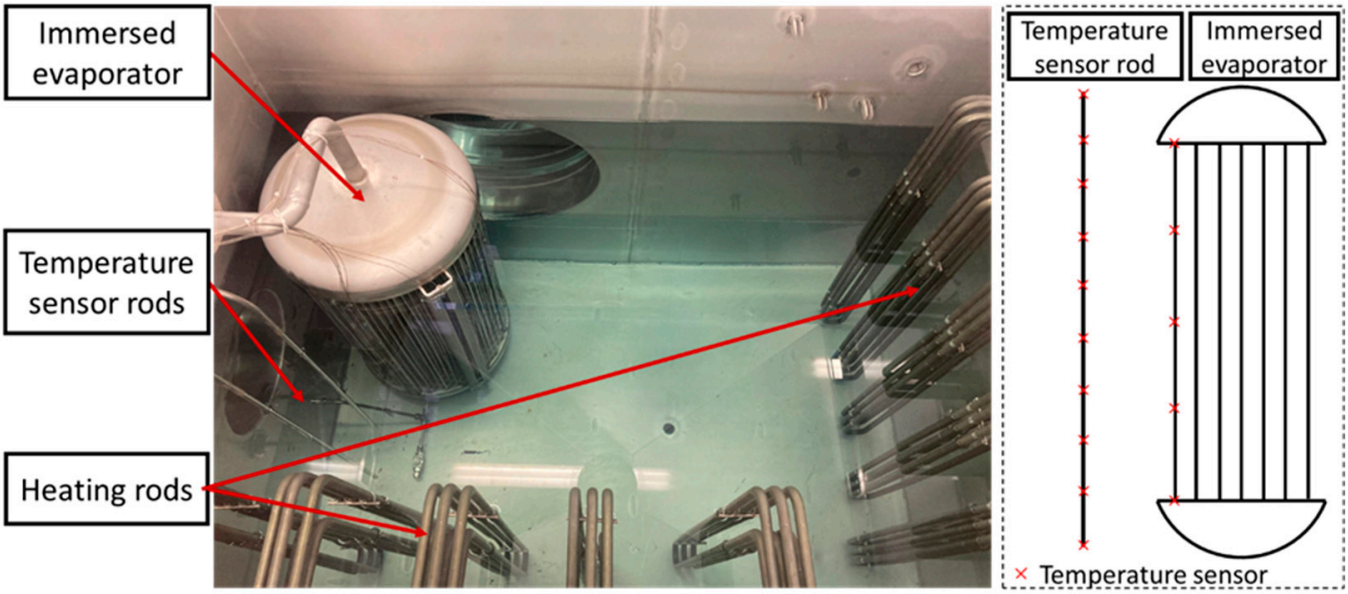

Figure 3. Boiling water tank.

2.2. Measurement

The characteristics of the measurement and data acquisition equipment are provided in Table 5. T-Type thermocouples are installed throughout the working fluid circuit, the water tank, and the cold source loops to monitor the temperatures across various components. Table 4 details the temperature sensors located on the outer tube wall of the evaporator. The working fluid circuit is equipped with absolute pressure sensors (APS) at the turbine inlet and outlet. Volume flow measurements in the cold circuit are performed using electromagnetic flow meters (EFMs), while the organic working fluid flow is measured with a Coriolis-type mass flow meter. The power generated by the turbine is measured with a power meter.

Table 5. Measurement characteristics.

Variable	Equipment	Range	Uncertainty
Electrical power	Wattmeter	0–3250 W	±0.3%
Volume flow (cold source)	EFM	0–2500 L/h	±0.33%
Mass flow rate (working fluid)	Coriolis	50–500 kg/h	±0.30%
Temperature	Thermocouple Type-T	−200–200 °C	±0.1 °C
Pressure	APS	0–7 bar	±1 %

2.3. Working Fluid

The working fluid is a key component in an ORC engine, as the engine's performance is highly dependent on its properties [23]. However, the selection of a working fluid is not exclusively determined by energetic considerations [24]. Multiple factors influence the choice, including the cold source temperature, hot source temperature, ambient conditions, performance, compatibility with turbine lubricants, ecological and environmental impact, ease of handling, availability, and cost [25,26]. In this study, Novec649™ and HFE7100 (both from 3M, Cergy Pontoise, France) were selected as working fluids. T-s diagrams of working fluids are presented in Figure 4, and their physical properties are summarized in Table 6.

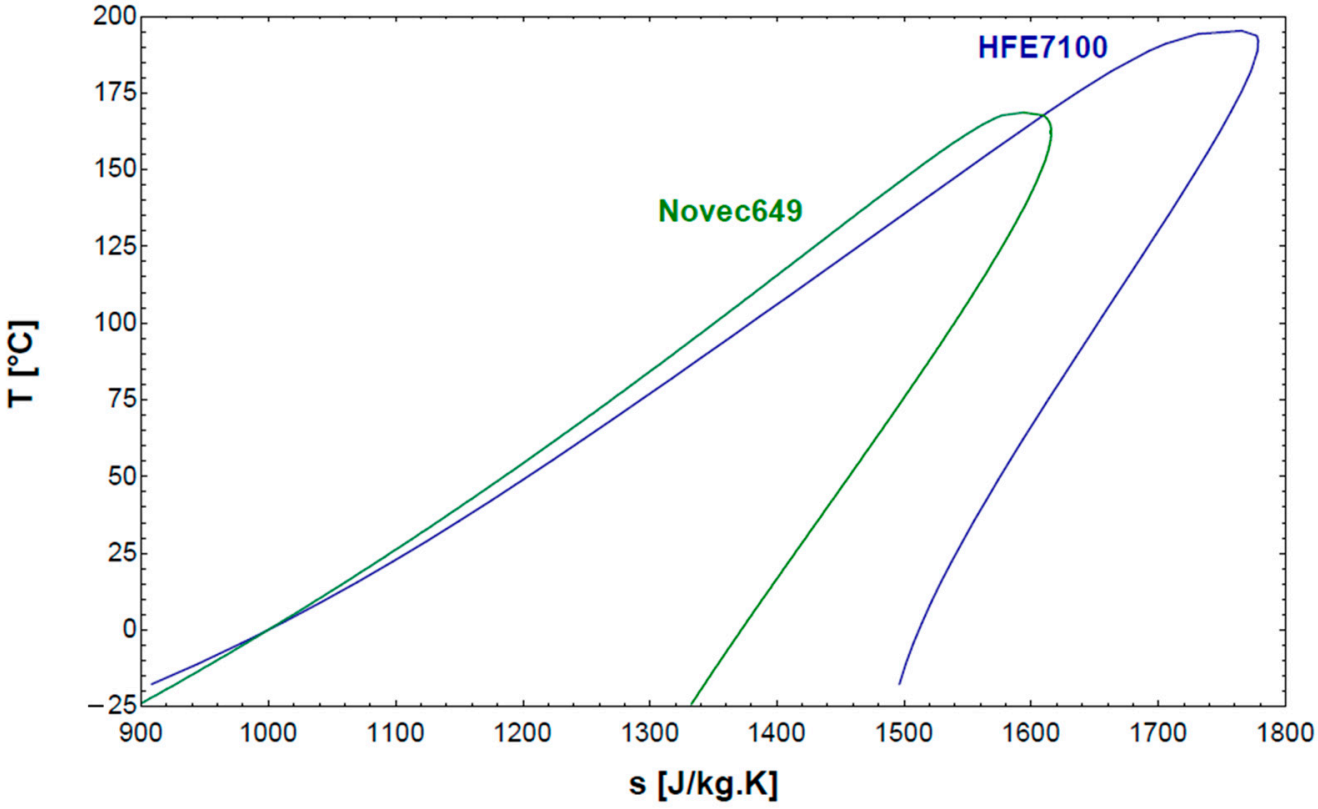

Figure 4. T-s diagram of Novec649™ and HFE7100.

Table 6. Main properties of the working fluids studied.

Properties	Units	Novec649™	HFE7100
Fluid type	[-]	Dry	Dry
Molar Mass	[g·mol^{-1}]	316	250
Saturation temperature at Patm	[°C]	49.1	61
Latent heat at Patm	[kJ·kg^{-1}]	88.1	116.4
Critical temperature	[C]	168.7	195.3
Saturation Pressure at 100 °C	[bar]	4.47	3.17
Critical Pressure	[bar]	18.7	22.3
Critical Density	[kg·m^{-3}]	606.8	555
ODP	[-]	0	0
GWP	[-]	1	320
Flammability	[-]	No	No
Toxicity	[-]	None	Low

Given the emphasis on reliability in this study, two working fluids were considered:

- HFE7100, a hydrofluoroether, is a replacement for CFC- and HCFC-type fluids. It was initially selected for its performance. In small-scale power production, around 1 kWe, studies by Kaczmarczyk and Żywica (2022), Jradi et al. (2014), and Kaczmarczyk (2021) achieved motor efficiencies of 5.97%, 5.7%, and 3.31%, respectively, using different types of expanders: a scroll expander, a radial turbine, and two scroll expanders in series [27–29]. As shown in Table 6, this fluid has a zero ozone depletion potential (ODP) and a relatively low Global Warming Potential (GWP) of approximately 320. Its low toxicity and non-flammability ensure user safety. With a saturation temperature of 61 °C at atmospheric pressure, the fluid undergoes depression when the ORC engine is stopped, ensuring retention within the system in case of leakage. Its saturation pressure at 100 °C is about 3.17 bar, which reduces the mechanical stress on ORC components. These characteristics suggest that HFE7100 is suitable for the intended application [30]. However, despite its relatively low GWP, it may face future regulatory restrictions.
- In anticipation of this, a second working fluid, Novec649™, with a GWP of 1, was also tested. Novec649™ shares some similarities with HFE7100 (zero ODP, dry fluid, non-flammability) but differs in certain aspects. Notably, there is a significant difference in their latent heat, as shown in Table 6. Novec649™ is a fluoroketone that is structurally and chemically similar to HFE. Under operating conditions with a hot source temperature below 120 °C, a cold source temperature of 40 °C, and an electrical output of 170 W, Dong and Jeong (2020) achieved a cycle efficiency of 4.5% [31]. Additionally, Scaccabarozzi et al. (2018) conducted a theoretical comparison of the performance of HFC and HFE fluids, indicating that Novec649™ ranks among the fluids with the highest cycle efficiency [32]. These performance metrics, coupled with its non-toxicity, non-flammability, and minimal environmental impact, position Novec649™ as an excellent candidate for use in ORC systems. Furthermore, like HFE7100, Novec649™ remains in a state of depression when the ORC engine is stopped, and its pressure at 100 °C does not exceed 4.5 bar. Given the limited power level and capacity of this study, these fluids are deemed suitable for the current application, though the requirements may differ for very large ORC plants.

3. Heat Exchangers Models

3.1. Condenser Model

The condenser's primary role is to condense the organic fluid with a specified degree of subcooling to mitigate any risk of cavitation in the pump. The condenser model is structured into three exchange zones, each corresponding to distinct physical phenomena (Figure 5).

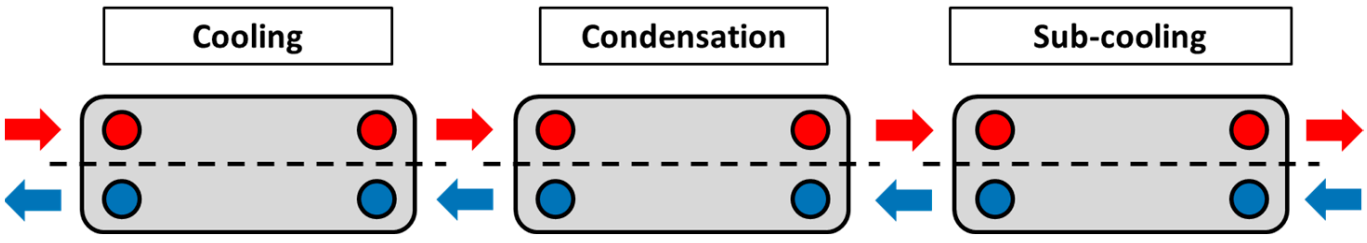

Figure 5. Modeling zones of the condenser (in red: working fluid; in blue: cold source fluid; arrows represent each fluid flow path; dots represent inlet and outlet sections).

Assuming that heat transfer between the working fluid and the cold source occurs with negligible thermal losses, the thermal balance for each zone of the condenser can be expressed using the Logarithmic Mean Temperature Difference (LMTD) method, as represented in Equations (1)–(3) for each zone of the condenser:

$$\dot{Q} = \dot{m}_c \cdot (h_{c,out} - h_{c,in}) \quad (1)$$

$$\dot{Q} = \dot{m_{wf}} \cdot \left(h_{wf,in} - h_{wf,out} \right) \quad (2)$$

$$\dot{Q} = U \cdot S \cdot \Delta T_{LM} \quad (3)$$

$\dot{Q}$ is the thermal power, and S represents the exchange area between the cold source and the working fluid. In the case of plate heat exchangers, this area is identical on both the fluid side and the source side. $\dot{m_c}$ is the mass flow rate of the cold source fluid, $\dot{m_{wf}}$ is the mass flow rate of the working fluid, h is the enthalpy, and U represents the overall heat transfer coefficient. This global heat transfer describes heat exchanges on the fluid and source sides as well as conduction through the wall:

$$\frac{1}{U} = \frac{1}{\alpha_c} + \frac{e}{\lambda} + \frac{1}{\alpha_{wf}} \quad (4)$$

e is the thickness of the plate between the source and the working fluid, λ is the material thermal conductivity, α_c is the cold source heat transfer coefficient, and α_{wf} is the working fluid heat transfer coefficient. The heat transfer coefficients appear in the form of a dimensionless parameter such as the following:

$$Nu = \alpha \cdot \frac{D_h}{\lambda} \quad (5)$$

Nu is the Nusselt number, D_h is the characteristic length, and λ is the fluid thermal conductivity.

3.1.1. One-Phase Heat Transfer Coefficient

In the plate condenser of the test bench, the cold source consists of chilled water at an inlet temperature set by a chiller unit, typically around 13 °C. The mass flow rate of the cold water is consistently nearly ten times higher than that of the organic working fluid. As previously mentioned, the working fluid remains in a single-phase state during both the heating and superheating stages.

In the case of single-phase flow within a plate heat exchanger, the Nusselt number can be defined according to the following equation [33]:

$$Nu = a \cdot Re^b \cdot Pr^{1/3} \quad (6)$$

Re is the Reynolds number, Pr is the Prandtl number, and a and b are constants depending on the precise geometry of the plate evaporator. These values are provided in Table 7. This correlation is used for both water and organic fluid.

Table 7. Constants for single-phase heat transfer in corrugated plate evaporators [34].

Reynolds	*a*	*b*
$50 < Re < 14,600$	0.347	0.653

3.1.2. Two-Phase Heat Transfer Coefficient

There are numerous heat transfer correlations for condensation in a plate condenser [35]. However, a comparative study of condensation correlations carried out on the same ORC engine with the same condenser concluded that the Shon correlation gave the best results [36,37].

The Shon correlation, as presented in Equation (7), was initially derived from experimental data using R-1233zd(e). Its validity range is $500 < Re_{eq} < 2500$ and $4.8 < Pr_l < 5.3$.

$$Nu_{Shon} = 2.337 \cdot Re_{eq}^{1.024} \cdot Re_{lo}^{-0.294} \cdot Bo_{eq}^{0.361} \cdot Pr_l^{0.333} \quad (7)$$

Re_{eq} is the equivalent Reynolds number (based on the equivalent mass flux), Re_{lo} is the liquid Reynolds number in two-phase flow, Bo_{eq} is the equivalent boiling number, and Pr_l is the Prandtl number in the liquid phase.

One of the objectives of this model is to demonstrate the reliability of the Organic Rankine Cycle (ORC) engine under specific off-design conditions. As previously mentioned, a particularly relevant scenario involves variations in the cold source temperature.

3.2. Evaporator Model

Similar to the condenser model, the numerical model for the immersed evaporator is divided into three distinct zones based on the fluid's state. These zones include a preheating section, an evaporation section, and a superheating section. This division into three zones is illustrated in Figure 6.

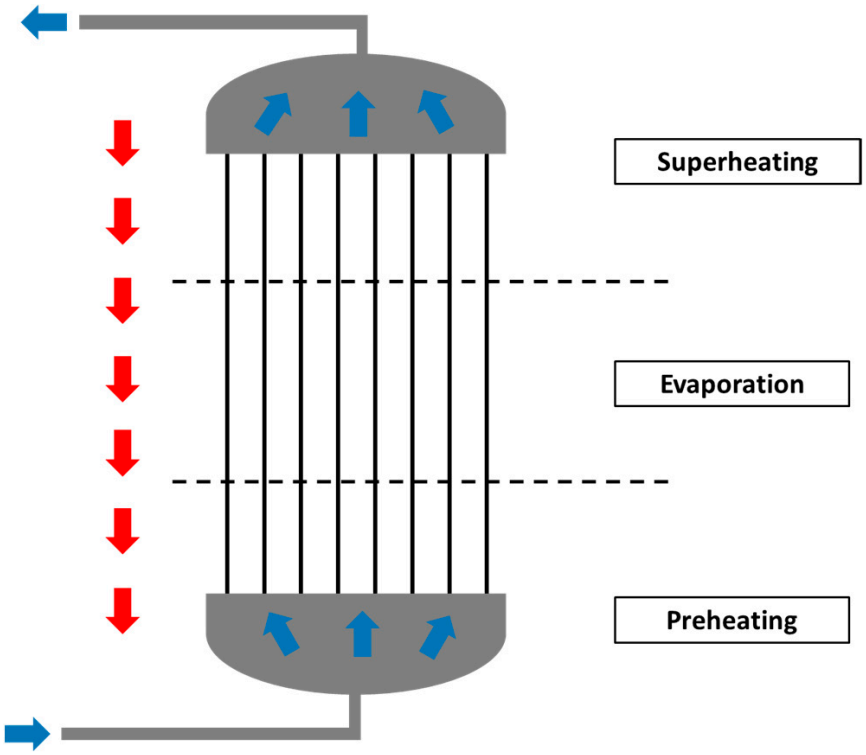

Figure 6. The segmentation of the immersed evaporator.

The configuration of the evaporator, which is immersed in the boiling tank, ensures that all heat exchange between the working fluid and the water occurs via convection. The balance Equations (8)–(10) for each zone of the immersed evaporator can be expressed as follows:

$$\dot{Q} = \dot{m}_c \cdot \left(h_{wf,out} - h_{wf,in} \right) \tag{8}$$

$$\dot{Q} = U \cdot S \cdot \Delta T_{LM} \tag{9}$$

$$\dot{Q} = \alpha_{water} \cdot S \cdot (T_{water} - T_w) \tag{10}$$

α_{water} is the water convective heat transfer coefficient, T_{water} is the temperature of the water near the wall, and T_w is the temperature of the wall outside the tube.

The method for resolving the balance equations follows the same approach outlined in the condenser section. The primary distinction lies in the correlations employed to calculate the heat exchange coefficients.

3.2.1. Natural Convection

The heat transfer regime outside the tubes in the boiling water tank is governed by natural convection, which is characterized by the Grashof number [38]. Assuming that the wall temperature remains constant for each zone of the evaporator, the Grashof number can be expressed as follows:

$$Gr = \rho^2 \cdot g \cdot \beta \cdot (T_{water} - T_w) \cdot \frac{D_{out,tube}^3}{\mu^2} \tag{11}$$

g is the acceleration due to gravity, β is the thermal expansion coefficient, $D_{out,tube}$ is the outer diameter of a tube of the evaporator, and μ is the dynamic viscosity.

The Rayleigh number is also useful to characterize the natural convection and to define the flow regime. It is defined as follows:

$$Ra = Gr \cdot Pr \tag{12}$$

The MARS Code (Multi-dimensional Analysis of Reactor Safety) approach was chosen to express the Nusselt number. MARS is a code developed by the Korea Atomic Energy Research Institute (KAERI) with the objective of providing a realistic analysis of thermo-hydraulic systems with multidirectional analysis capabilities [39]. The correlation used to calculate the natural convection heat transfer coefficient for vertical tubes is the Churchill and Chu correlation (1975) [40,41]:

$$Nu = \left(0.825 \frac{0.387 Ra^{\frac{1}{6}}}{\left(1 + \left(\frac{0.492}{Pr}\right)^{\frac{9}{16}}\right)^{\frac{8}{27}}} \right)^2 \tag{13}$$

where $Ra > 10^{-1}$.

3.2.2. One-Phase Heat Transfer Coefficient

In the liquid phase, the Reynolds number typically remains below 2300, indicating a laminar flow regime. The literature suggests treating the Nusselt number as a constant under these conditions, provided that the length of the tube is sufficient to establish stable velocity and temperature profiles. Assuming a uniform heat flux at the wall, the Nusselt number in the liquid phase can be expressed as follows [42]:

$$Nu_l = 4.36 \tag{14}$$

In single-phase vapor, the flow regime in the tubes becomes turbulent. The Nusselt number value is calculated using the Dittus–Boelter correlation (1930) [42,43]:

$$Nu_v = 0.0243 \cdot Re_v^{0.8} \cdot Pr^{0.4} \tag{15}$$

Re_{vap} is the Reynolds number in the vapor phase.

3.2.3. Two-Phase Heat Transfer Coefficient

Warrier et al. (2002) developed a correlation that depends only on the boiling number and the vapor quality of the fluid. This correlation, based on the experimental results of organic working fluid (FC-84) within small test sections, is expressed in the following form [44]:

$$\alpha_{Warrier} = \left(1 + 6 \cdot Bo^{\frac{1}{16}} - 5.3 \cdot (1 - 855 \cdot Bo) \cdot x^{0.65}\right) \cdot \alpha_{lo} \tag{16}$$

Bo is the boiling number, x is the vapor quality, and α_{lo} is the heat transfer coefficient in the liquid phase.

This correlation provides satisfactory results for the nominal operating point with Novec649™, demonstrating a ratio of 1.11 between the theoretical and experimental heat transfer coefficients. However, during off-nominal operating tests with HFE7100—particularly those resulting in incomplete evaporation—this correlation tends to underestimate the heat transfer coefficient. To address this limitation, we have modified the correlation to enhance the contribution of vapor quality. The revised correlation was derived empirically:

$$\alpha_{\text{modified\_Warrier\_correlation}} = \left(A - B * Bo^2 + C \cdot Bo * (0.5 - x) + D \cdot \left(Bo * (0.5 - x)\right)^2\right) \cdot \alpha_{lo} \quad (17)$$

where $A = 5.4846, B = 1.4602 \times 10^7, C = 41,413.5,$ *and* $D = 4.5738 \times 10^8$.

4. Results and Discussion

4.1. ORC Engine Results in Nominal Configuration

The overall efficiency of the engine during nominal operation with Novec649™ is approximately 2% (see Table 8). This low efficiency can be attributed to the moderate hot source temperature and the small size of the engine, which necessitated the use of a partial admission machine. Detailed information on the turbine type and its efficiency can be found in another article [45]. It is anticipated that a projected full-scale machine (i.e., one without partial admission) would achieve a higher efficiency. However, the low efficiency of the overall system is not a critical issue, as the amount of heat that can be recovered significantly exceeds the heat required for the ORC to function effectively (refer to Tables 1 and 2).

Table 8. The ORC nominal point (Novec649^{TM}).

Specification	Unit	Data
Electrical power	Watts	138
Overall efficiency	%	1.87
Turbo generator efficiency (electric)	%	16
Exergetic efficiency	%	8.17
Pressure rate	[-]	7.4
Temperature of hot source	°C	≈100
Cold source temperature	°C	13

This nominal point corresponds to the reference and maximal conditions for the tested engine.

These results under nominal operating conditions demonstrate the technical feasibility of coupling a boiling water tank with an ORC engine. However, beyond merely illustrating the feasibility of this coupling under nominal operation, one of the main objectives of this article is to examine the operation of this coupling in various off-nominal situations. The component models will be validated over a wide range of applications by testing under these conditions.

Thus, several experimental campaigns focusing on degraded operation tests and alternative configurations have been carried out:

- The variation in the cold source temperature;
- The variation in the power and positioning of heating elements in the tank;
- The use of different organic working fluids.

These experimental campaigns will provide valuable insights for validating the condenser and evaporator models under both nominal and off-nominal conditions.

4.2. Variation in the Cold Source Temperature

This experimental campaign investigates the variation in cold source temperatures from 13 °C to 33 °C. Figure 7 illustrates the relationship between the electrical output of the ORC engine and the cold source temperature. It is evident that the power generated by the engine decreases as the cold source temperature increases: specifically, a 20 °C rise results in a reduction in more than half of the electrical power output. This decrease in efficiency aligns qualitatively with Carnot's theory, which highlights the impact of temperature differences between hot and cold sources on the overall efficiency of a thermodynamic system. Notably, the efficiency of the setup declines faster than predicted by the Carnot efficiency.

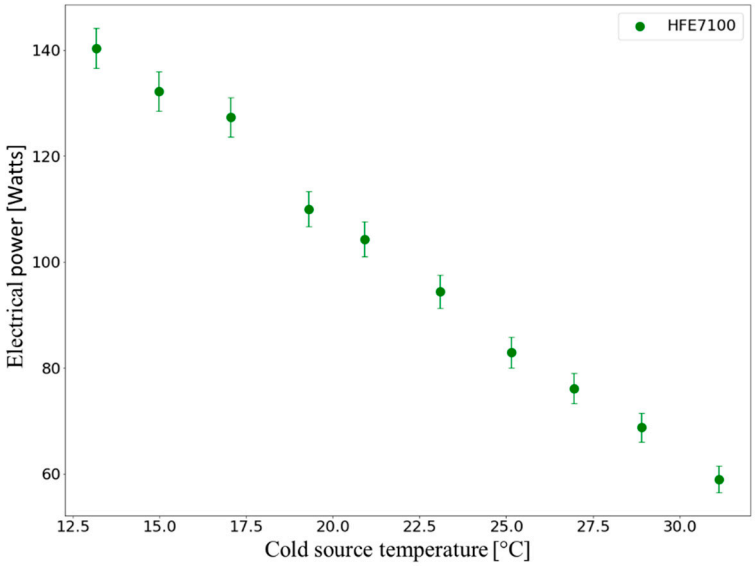

Figure 7. The variation in electrical power output as a function of cold source temperature.

To further understand this behavior, examining the variation in the exergy efficiency is crucial, as the exergy efficiency can be expressed as the ratio of the energy efficiency to Carnot efficiency. Figure 8 depicts the variation in the exergy efficiency, which clearly demonstrates a downward trend.

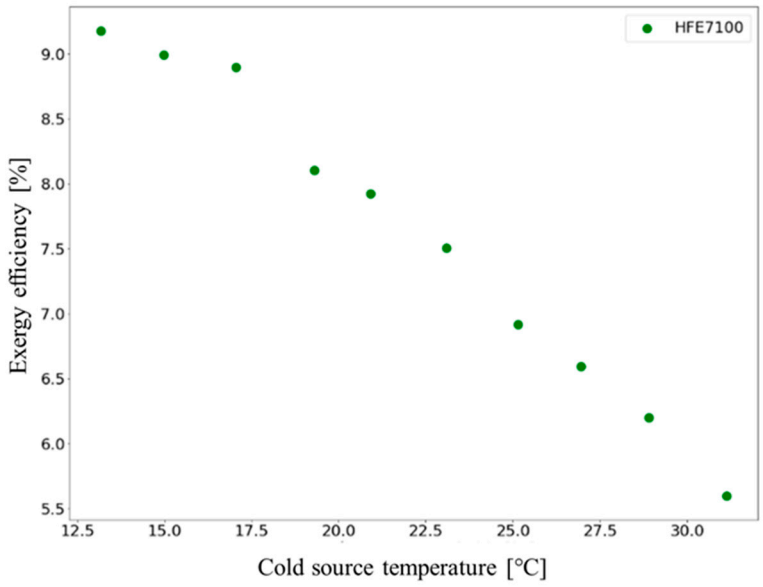

Figure 8. The variation in exergy efficiency as a function of cold source temperature.

One plausible hypothesis for this rapid decline in efficiency is the corresponding decrease in turbo-generator efficiency linked to the reduction in electrical power production. Indeed, a 20 °C increase in cold source temperature leads to a drop in turbo-generator efficiency from 16% to 8%. As the cold source temperature rises, the pressure ratio decreases, thereby reducing the intrinsic efficiency of the turbine.

This off-design study on cold source temperature quantitatively illustrates the effect of varying cold temperatures on electrical production without any intervention or control. Therefore, during the scaling process, the cold source temperature will be a fundamental factor in designing system components.

This campaign has yielded experimental results that can effectively validate the condenser model. Figure 9 presents a comparison between the condenser model predictions and the experimental results. The model demonstrates the capability to accurately represent heat exchanges within a margin of ±5% in power, applicable to both nominal point tests and off-design conditions.

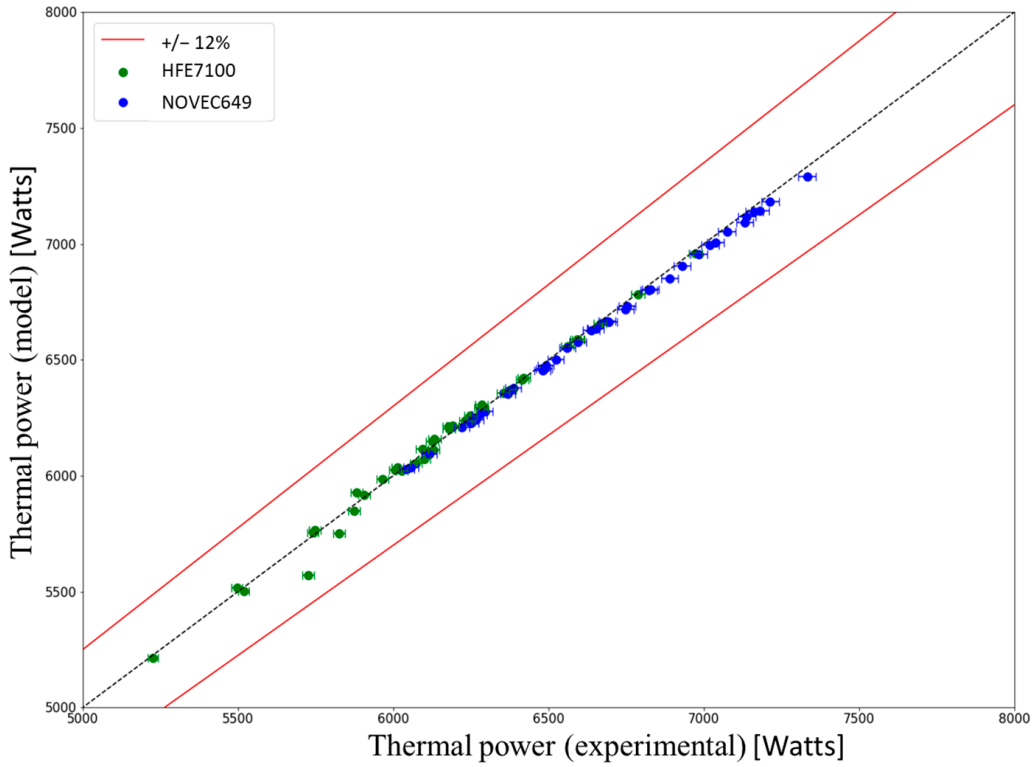

Figure 9. The measured condenser thermal power vs that predicted by the model.

The experimental study examining the variation in the cold source temperature enabled us to quantify the reduction in electrical production and efficiency as a function of temperature in the absence of any active control measures. The conclusions drawn from this study highlight the significant impact of cold source temperature on the thermodynamic cycle's performance. These findings emphasize the necessity of incorporating the maximum cold source temperature when modeling the ORC system at full scale, ensuring coverage of all potential operating regimes. In designing full-scale systems, it is crucial to include a sufficient margin to accommodate extreme temperature scenarios.

4.3. Variation in Operating Conditions of the Hot Source

A primary focus of the experimental campaign is the positioning of the immersed evaporator within the tank: specifically, whether its location between the heating elements influences system performance. Additionally, we aim to explore the relationship between the heating rod power and the engine's power output. Another objective is to validate the model

regarding the thermal exchange between the water tank and the immersed evaporator for both organic fluids. The modification of Warrier's correlation, as detailed in Section 3.2.1, has been established through results obtained via a "semi-empirical methodology".

To address these questions, we conducted an initial test campaign investigating heating power and the position of the heating rods in the tank. The heating rod power varied from 20 to 80 kW for both heating zones, while the evaporator's thermal power did not exceed 8 kW in any test. Two heating zones were set up for the experiment, as presented in Figure 2: Zone 1 corresponds to the heating rods nearest to the heat exchanger, while Zone 2 corresponds to those further away.

Figure 10 illustrates the electrical power produced as a function of the heating rod power. It is evident that at a hot source power of 20 kW, electrical production is approximately 100 W for the closest rods compared to about 120 W for the furthest rods. This power increases to a plateau of around 140 W, achieved with rod powers of 40 kW for the closest rods and 60 kW for the furthest rods. The graph indicates a correlation between the rod power and the turbine power output up to a heating power of about 60 kW. Beyond this threshold, electrical production stabilizes, with the furthest rods yielding a slightly higher power output. This surplus can be attributed to a convective cell that enhances the velocity and flow rate of the descending water mass, which is particularly pronounced with the furthest rods due to the tank's geometry and the alignment of the heating rods with the evaporator.

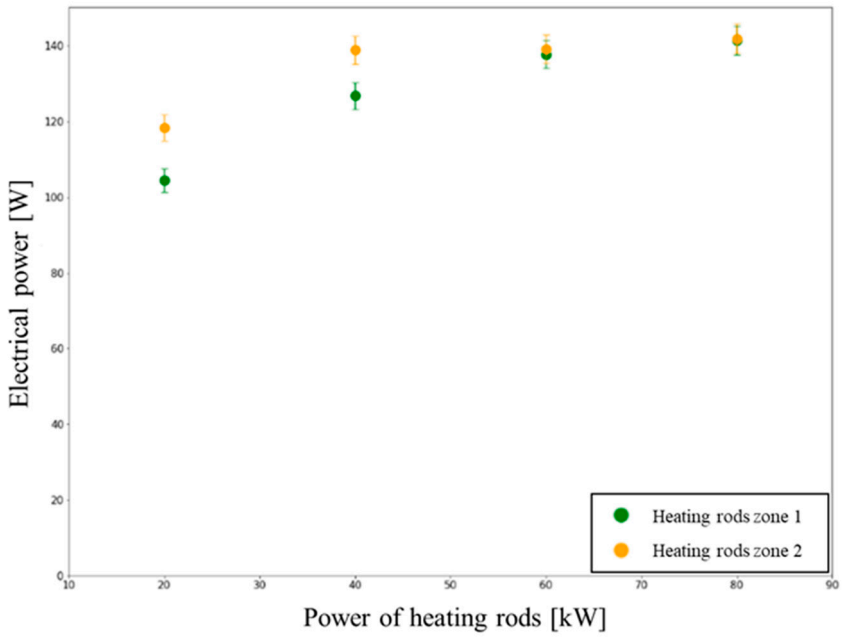

Figure 10. The electrical power produced based on the power of the heating rods.

The value of 60 kW marks the point at which the dependency on heating zone power is no longer a factor. Above this threshold, the turbine power output no longer correlates with the position of the heating elements in the tank. When the ratio of the ORC evaporator power to heating rod power exceeds approximately 10 (with an evaporator thermal power of around 6 kW and heating rod power at 60 kW), no correlation exists between the engine's electrical production and the power/position of the heating elements. These results suggest that, when the ratio falls below 0.1, the overall system behavior remains unaffected by this ratio.

Regarding the validity of the evaporator model, Figure 11 demonstrates that utilizing Warrier's correlation, as detailed in Section 3.2.1, in conjunction with the overall model for preheating and superheating, enables accurate modeling of the evaporator within ±12% in thermal power for both HFE7100 and Novec649^{TM}. This model effectively describes both complete and incomplete organic working fluid evaporation, which is critical for

designing a full-scale system with an adequate safety margin. Incomplete evaporation poses a well-known risk of turbine underproduction and potential turbine failure if the vapor's thermodynamic quality is significantly below 1. A more in-depth analysis of this phenomenon is the focus of a separate article [45]. However, it is important to note that the modified Warrier correlation may not yield satisfactory results for all working fluids, even though Novec649™ and HFE7100 exhibit notably different characteristics, particularly in terms of latent heat (refer to Table 6).

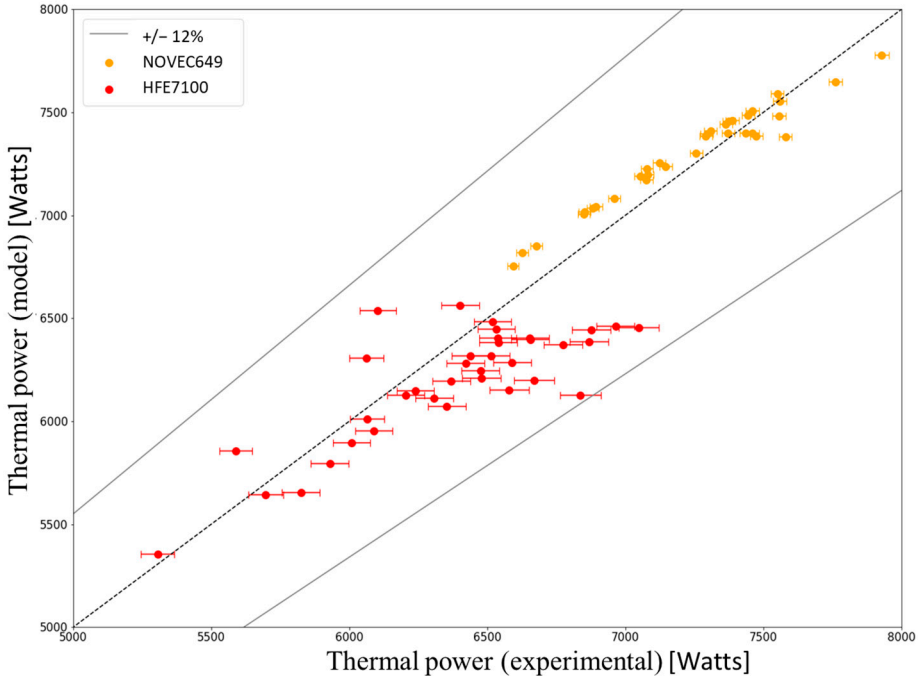

Figure 11. Evaporator power theoretical model as a function of experimental results.

5. Conclusions

This study investigates a waste heat recovery process utilized in a specific autonomous safety system for an advanced nuclear reactor. The research is driven by the potential to harness a portion of the energy stored in an existing volume of boiling water as a heat source for an Organic Rankine Cycle (ORC). The goal of this preliminary design phase was to experimentally assess, at a reduced scale, the feasibility of leveraging heat from a boiling water tank to power an ORC engine via an immersed evaporator.

Initially, the research focused on the system's nominal operation using Novec649™. Subsequently, three off-design configurations were examined: variations in cold source temperature, the impact of the alternative positioning of the immersed evaporator within the tank, and the choice of the ORC working fluid. The experimental campaign quantified the reduction in the power output associated with an increase in the cold source temperature (without any control measures), revealing that a temperature rise of 20 °C (from 15 °C to 35 °C) results in more than a 50% decrease in electrical power generation. Furthermore, it was demonstrated that, once the heating power in the tank surpasses ten times the thermal power recovered by the ORC system, the position of the evaporator and further increases in this power disparity do not significantly affect engine output.

These test campaigns successfully validated the condenser model, achieving a power deviation of ±5% for both nominal and off-design conditions. Additionally, they led to the development of an evaporation correlation based on Warrier's correlation (2002) [44]. This semi-empirical approach allowed for the accurate description of heat transfer at the immersed evaporator within ±12% for tests conducted under both nominal and off-design scenarios, using two different ORC working fluids: Novec649™ and HFE7100.

This experimental validation marks a crucial step toward scaling up the entire system. Future investigations will consider other working fluids and explore additional off-design situations, including the fouling or degradation of heat exchangers and variations in working fluid charge, such as fluid loss scenarios.

Author Contributions: Conceptualization, G.L., N.T., N.C. and F.M.; methodology, G.L., N.T. and N.C.; formal analysis, G.L., N.T. and N.C.; investigation, G.L., N.T., N.C. and B.P.; writing—original draft preparation, G.L., N.T. and N.C.; writing—review and editing, G.L., N.T., N.C., B.P. and F.M.; supervision, N.T., N.C. and F.M. All authors have read and agreed to the published version of the manuscript.

Funding: This research received funding from the Atomic Energy and Alternative Energies Commission (CEA) and Electricité de France (EDF).

Data Availability Statement: The datasets presented in this article are not readily available because the data are part of an ongoing study.

Acknowledgments: The authors would like to express their gratitude to the Atomic Energy and Alternative Energies Commission (CEA) and Electricité de France (EDF).

Conflicts of Interest: The authors declare no conflicts of interest.

Nomenclature

Symbols

Bo	boiling number	[-]
d	tube diameter	[m]
e	plate thickness	[m]
g	acceleration of gravity	[m/s^2]
Gr	Grashof number	[-]
h	enthalpy	[J/kg]
$\dot{m}$	mass flow rate	[kg/s]
Nu	Nusselt number	[-]
Pr	Prandtl number	[-]
$\dot{Q}$	thermal power	[Watts]
Re	Reynolds number	[-]
S	surface	[m^2]
T	temperature	[K]
U	overall heat transfer coefficient	[W/m^2·K]
x	vapor quality	[-]

Greek letters

α	heat transfer coefficient	[W/m^2·K]
β	coefficient of thermal expansion	[K^{-1}]
λ	thermal conductivity	[W/m·K]
μ	dynamic viscosity	[Pa·s]
ρ	density	[kg/m^3]

Subscripts

d	diameter
eq	equivalent
exp	experimental
h	hot
l	liquid
Lo	liquid only
sp	single-phase
tp	two-phase
v	vapor
w	wall
wf	working fluid

Glossary

EES	engineering equation solver
GWP	global warming potential
HX	heat exchanger
IRWST	in-containment refueling water storage tank
NPSH	net positive suction head
NPP	nuclear power plants
ODP	ozone depletion potential
PRHRS	passive residual heat removal system
SACO	safety condenser
SBO	station blackouts
SG	steam generator
SSPRHRS	secondary side passive residual heat removal system

References

1. World Nuclear Association. *Nuclear Power Today | Nuclear Energy*; World Nuclear Association: London, UK, 2022; Available online: https://www.world-nuclear.org/information-library/current-and-future-generation/nuclear-power-in-the-world-today.aspx (accessed on 28 November 2022).
2. IAEA. *Energy, Electricity and Nuclear Power Estimates for the Period up to 2050*; International Atomic Energy Agency: Vienna, Austria, 2022; Available online: https://linkinghub.elsevier.com/retrieve/pii/0140670195951326 (accessed on 28 November 2022).
3. Skillman, G.R.; Rempe, J.L. The Three Mile Island Unit 2 Accident. In *Encyclopedia of Nuclear Energy*; Greenspan, E., Ed.; Elsevier: Oxford, UK, 2021; pp. 17–29. [CrossRef]
4. Sich, A.R. The Chernobyl Nuclear Power Plant Unit-4 Accident. In *Encyclopedia of Nuclear Energy*; Greenspan, E., Ed.; Elsevier: Oxford, UK, 2021; pp. 30–52. [CrossRef]
5. IAEA (Ed.) *The Fukushima Daiichi Accident*; International Atomic Energy Agency: Vienna, Austria, 2015.
6. Olatubosun, S.A.; Smidts, C. Reliability analysis of passive systems: An overview, status and research expectations. *Prog. Nucl. Energy* **2022**, *143*, 104057. [CrossRef]
7. Li, J.; Qi, Z.; Cao, K.; Liu, M.; Yang, Z.; Xiao, Y.; Xiong, Z.; Gu, H. Experimental investigation on the heat removal capacity of secondary side passive residual heat removal system for an integrated reactor. *Appl. Therm. Eng.* **2022**, *204*, 117973. [CrossRef]
8. Estévez-Albuja, S.; Jiménez, G.; Vázquez-Rodríguez, C. AP1000 IRWST numerical analysis with GOTHIC. *Nucl. Eng. Des.* **2021**, *372*, 110991. [CrossRef]
9. Li, Y.Q.; Chang, H.J.; Ye, Z.S.; Fang, F.F.; Shi, Y.; Yang, K.; Cui, M.T. Analyses of ACME integral test results on CAP1400 small-break loss-of-coolant-accident transient. *Prog. Nucl. Energy* **2016**, *88*, 375–397. [CrossRef]
10. Sun, D.C.; Li, Y.; Xi, Z.; Zan, Y.F.; Li, P.Z.; Zhuo, W.B. Experimental evaluation of safety performance of emergency passive residual heat removal system in HPR1000. *Nucl. Eng. Des.* **2017**, *318*, 54–60. [CrossRef]
11. Baek, J.Y.; Lee, S.; Kim, G.; Lee, J.I. Application of the passive turbocharger to PRHRS in integral PWR type SMR with an sCO_2 power cycle. *Ann. Nucl. Energy* **2025**, *210*, 110874. [CrossRef]
12. IRSN. *Éléments de Sûreté Nucléaire-Les Réacteurs de Recherche*; EDP Sciences: Les Ulis, France, 2019. [CrossRef]
13. Singh, K.P.; Sound, H.; Rampall, I.; Hill, C.; Rajkumar, J. Autonomous Self-Powered System for Removing Thermal Energy from Pools of Liquid Heated by Radioactive Materials and Method of the Same. U.S. Patent 9,803,510, 31 October 2017.
14. Tatli, E.; Belechak, J.G.; Lu, B.; Stansbury, C.; Guler, C.; Ostrosky, M.J. Power Generation from Decay Heat for Spent Nuclear Fuel Pool Cooling and Monitoring. U.S. Patent 2013/0028365A1, 31 January 2013.
15. Astolfi, M. 3-Technical options for Organic Rankine Cycle systems. In *Organic Rankine Cycle (ORC) Power Systems*; Macchi, E., Astolfi, M., Eds.; Woodhead Publishing: Sawston, UK, 2017; pp. 67–89. [CrossRef]
16. Obi, J.B. State of Art on ORC Applications for Waste Heat Recovery and Micro-cogeneration for Installations up to 100 kWe. *Energy Procedia* **2015**, *82*, 994–1001. [CrossRef]
17. Tauveron, N.; Colasson, S.; Gruss, J.-A. Available systems for the conversion of waste heat to electricity. In Proceedings of the ASME 2014 International Mechanical Engineering Congress and Exposition, Montreal, QB, Canada, 14–20 November 2014. [CrossRef]
18. Wieland, C.; Dawo, F.; Schifflechner, C.; Astolfi, M. Market report on organic rankine cycle power systems: Recent developments and outlook. In Proceedings of the 6th International Seminar on ORC Power Systems, Munich, Germany, 11–13 October 2021.
19. Kim, S.-M.; Mudawar, I. Universal approach to predicting saturated flow boiling heat transfer in mini/micro-channels–Part II. Two-phase heat transfer coefficient. *Int. J. Heat Mass Transf.* **2013**, *64*, 1239–1256. [CrossRef]
20. Cour des Comptes. Adaptation-du-Parc-de-Reacteurs-Nucleaires-au-Changement-Climatique. March 2021. Available online: https://www.ccomptes.fr/system/files/2023-03/20230321-Adaptation-du-parc-de-reacteurs-nucleaires-au-changement-climatique_0.pdf (accessed on 29 August 2023).
21. IRSN. *Réacteurs Électronucléaires–EDF–Grand Chaud–Retour d'Expérience de la Canicule de l'Été 2019*; EDP Sciences: Les Ulis, France, January 2020; Available online: https://www.irsn.fr/sites/default/files/documents/expertise/avis/2020/Avis-IRSN-2020-00010.pdf (accessed on 29 August 2023).
22. Bae, B.-U.; Yun, B.-J.; Kim, S.; Kang, K.H. Design of condensation heat exchanger for the PAFS (Passive Auxiliary Feedwater System) of APR+ (Advanced Power Reactor Plus). *Ann. Nucl. Energy* **2012**, *46*, 134–143. [CrossRef]
23. Stijepovic, M.Z.; Linke, P.; Papadopoulos, A.I.; Grujic, A.S. On the role of working fluid properties in Organic Rankine Cycle performance. *Appl. Therm. Eng.* **2012**, *36*, 406–413. [CrossRef]
24. Chen, H.; Goswami, D.Y.; Stefanakos, E.K. A review of thermodynamic cycles and working fluids for the conversion of low-grade heat. *Renew. Sustain. Energy Rev.* **2010**, *14*, 3059–3067. [CrossRef]
25. Babatunde, A.F.; Sunday, O.O. A Review of Working Fluids for Organic Rankine Cycle (ORC) Applications. *IOP Conf. Ser. Mater. Sci. Eng.* **2018**, *413*, 012019. [CrossRef]
26. Quoilin, S.; Broek, M.V.D.; Declaye, S.; Dewallef, P.; Lemort, V. Techno-economic survey of Organic Rankine Cycle (ORC) systems. *Renew. Sustain. Energy Rev.* **2013**, *22*, 168–186. [CrossRef]
27. Kaczmarczyk, T.Z.; Żywica, G. Experimental research of a micropower volumetric expander for domestic applications at constant electrical load. *Sustain. Energy Technol. Assess.* **2022**, *49*, 101755. [CrossRef]
28. Jradi, M.; Li, J.; Liu, H.; Riffat, S. Micro-scale ORC-based combined heat and power system using a novel scroll expander. *Int. J. Low-Carbon Technol.* **2014**, *9*, 91–99. [CrossRef]

29. Zygmunt Kaczmarczyk, T. Experimental research of a small biomass organic Rankine cycle plant with multiple scroll expanders intended for domestic use. *Energy Convers. Manag.* **2021**, *244*, 114437. [CrossRef]
30. Landelle, N.; Tauveron, P.; Haberschill, R.; Revellin, S. Colasson, Performance Evaluation and Comparison of Experimental Organic Rankine Cycle Prototypes from Published Data. *Energy Procedia* **2017**, *105*, 1706–1711. [CrossRef]
31. Dong, H.-W.; Jeong, J.-W. Design and preliminary results of organic rankine cycle for liquid desiccant system. *Appl. Therm. Eng.* **2020**, *178*, 115596. [CrossRef]
32. Scaccabarozzi, R.; Tavano, M.; Invernizzi, C.M.; Martelli, E. Comparison of working fluids and cycle optimization for heat recovery ORCs from large internal combustion engines. *Energy* **2018**, *158*, 396–416. [CrossRef]
33. GRETh. TM11-Pertes de Pression et Transfert de Chaleur dans des Canaux Rectangulaires Corrugués. June 1999. Available online: https://greth.fr/tm11-pertes-de-pression-et-transfert-de-chaleur-dans-des-canaux-rectangulaires-corrugues/ (accessed on 16 July 2023).
34. Hugonnot, P. Etude Locale de l'Écoulement et Performances Thermohydrauliques à Faible Nombre de Reynolds d'un Canal Plan Corrugue-Applications Aux Échangeurs de Chaleur à Plaques. 1989. Available online: https://greth.fr/etude-locale-de-lecoulement-et-performances-thermohydrauliques-a-faible-nombre-de-reynolds-dun-canal-plan-corrugue-applications-aux-echangeurs-de-chaleur-a-plaques/ (accessed on 16 July 2023).
35. Tao, X.; Infante Ferreira, C.A. Heat transfer and frictional pressure drop during condensation in plate heat exchangers: Assessment of correlations and a new method. *Int. J. Heat Mass Transf.* **2019**, *135*, 996–1012. [CrossRef]
36. Blondel, Q.; Tauveron, N.; Lhermet, G.; Caney, N. Zeotropic mixtures study in plate heat exchangers and ORC systems. *Appl. Therm. Eng.* **2023**, *219*, 119418. [CrossRef]
37. Shon, B.H.; Jung, C.W.; Kwon, O.J.; Choi, C.K.; Tae Kang, Y. Characteristics on condensation heat transfer and pressure drop for a low GWP refrigerant in brazed plate heat exchanger. *Int. J. Heat Mass Transf.* **2018**, *122*, 1272–1282. [CrossRef]
38. Leleu, R. Transferts de chaleur. *Opér. Unit. Génie Réact. Chim.* **1992**, *1*, J1080. [CrossRef]
39. Chung, B.D.; Kim, K.D.; Bae, S.W.; Jeong, J.J.; Lee, S.W.; Hwang, M.K.; Yoon, C. *MARS Code Manual Volume I: Code Structure, System Models, and Solution Methods*; Korea Atomic Energy Research Institute: Daejeon, Republic of Korea, 2010; p. 620.
40. Churchill, S.W.; Chu, H.H.S. Correlating equations for laminar and turbulent free convection from a vertical plate. *Int. J. Heat Mass Transf.* **1975**, *18*, 1323–1329. [CrossRef]
41. Jeong, J.-J.; Ha, K.S.; Chung, B.D.; Lee, W.J. Development of a multi-dimensional thermal-hydraulic system code, MARS 1.3.1. *Ann. Nucl. Energy* **1999**, *26*, 1611–1642. [CrossRef]
42. GRETh. TM2-Transfert de Chaleur dans les Tubes de Section Circulaire. November 2003. Available online: https://greth.fr/tm2-transfert-de-chaleur-dans-les-tubes-de-section-circulaire/ (accessed on 25 July 2023).
43. Dittus, F.W.; Boelter, L.M.K. Heat transfer in automobile radiators of the tubular type. *Int. Commun. Heat Mass Transf.* **1985**, *12*, 3–22. [CrossRef]
44. Warrier, G.R.; Dhir, V.K.; Momoda, L.A. Heat transfer and pressure drop in narrow rectangular channels. *Exp. Therm. Fluid Sci.* **2002**, *26*, 53–64. [CrossRef]
45. Lhermet, G.; Tauveron, N.; Caney, N.; Blondel, Q.; Morin, F. A Recent Advance on Partial Evaporating Organic Rankine Cycle: Experimental Results on an Axial Turbine. *Energies* **2022**, *15*, 7559. [CrossRef]